WITH THE LAYER-DEPENDENT tunability of their optical band gap in the near-infrared (IR) to visible spectrum, transition metal dichalcogenides (TMDs), including molybdenum disulfide (MoS_2) and tungsten disulfide (WS_2), exhibit strong light–matter interactions, making them suitable as absorber layers for optoelectronic devices. Currently, the WS_2-based solar cells are fabricated via micromechanical/chemical exfoliation or transfer of two-dimensional (2-D) WS_2 layers onto conventional three-dimensional (3-D) bulk semiconductors, which poses a challenge for large-scale integrations and consequent device performances.

We report a transfer-free chemical vapor deposition (CVD) process for the growth of semiconducting WS_2 on p-type silicon (p-Si) substrates to build WS_2/p-Si heterojunction solar cells with a fill factor (FF) of 26%. The photoresponse and spectral response (quantum efficiency) of the WS_2/Si solar devices reveal junction characteristics such as trapped states and wavelength-dependent recombination mechanisms. The external quantum efficiency (EQE) of >60% is observed near the red and far-IR region, corresponding to the device's high photon absorption regime with a high diffusion length of the minority charge carriers. The present study opens avenues for the direct integration of the CVD-grown 2-D semiconducting WS_2 layers with Si-based vertical and lateral heterojunctions for efficient nano- and optoelectronic devices.
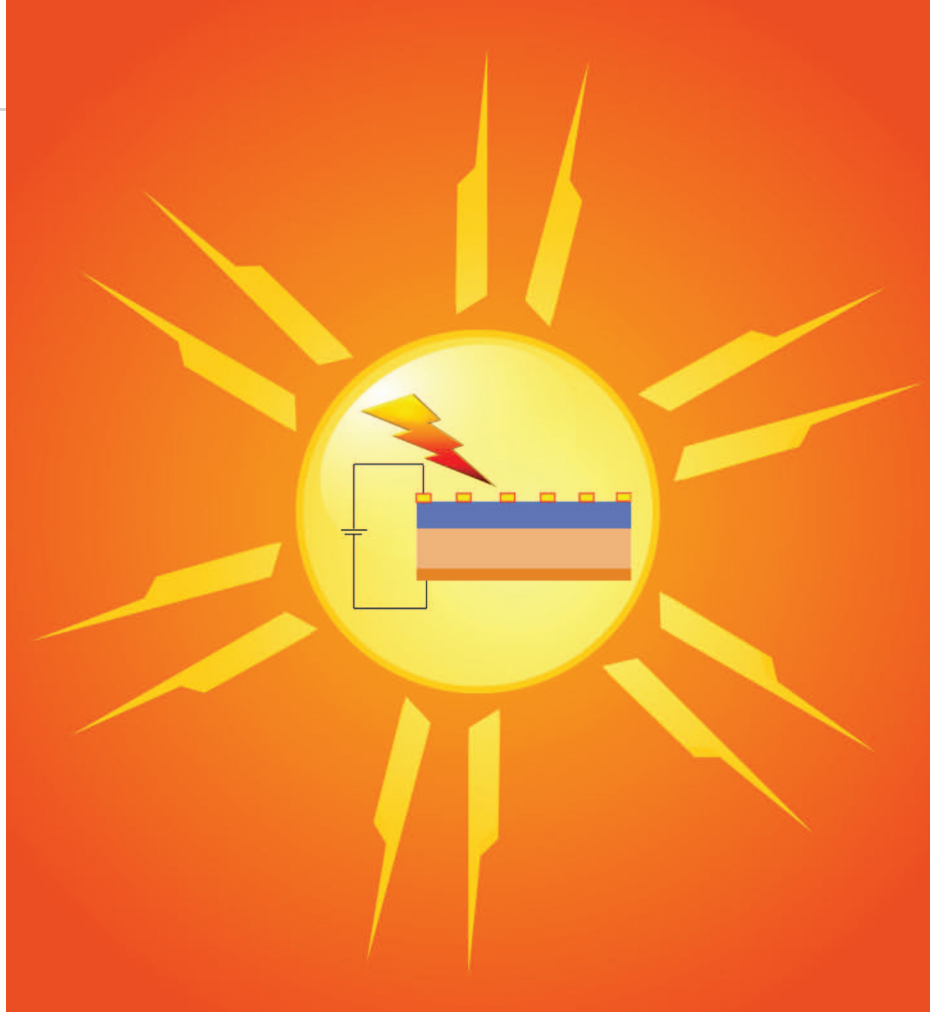
SUN—©GRAPHIC STOCK

WS2/Silicon Heterojunction Solar Cells

A CVD process for the fabrication of WS2 films on p-Si substrates for photovoltaic and spectral responses.

SANJAY BEHURA, KAI-CHIH CHANG, YU WEN, ROUSAN DEBBARMA, PHONG NGUYEN, SONGWEI CHE, SHIKAI DENG, MICHAEL R. SEACRIST, AND VIKAS BERRY

THE USE OF 2-D NANOMATERIALS IN PV DEVICES

Conventional energy sources, such as fossil fuels, are becoming depleted, thus demanding fast and steady implementation of renewable energy. The solar photovoltaic (PV) energy conversion contributes significantly to our total renewable energy resources and is primarily dependent on Si-based P–N homojunction solar cells. However, these solar cells are not cost effective, and their efficiency is restricted by the Shockley–Queisser limit [1]. More recently, 2-D nanomaterials, due to their unique optical, electronic, and mechanical properties, have shown promise for the development of cost-effective and efficient PV devices via integration with conventional bulk semiconductors [2], [3]. In this regard, TMDs, including MoS_2 and WS_2, are attractive because of their ultrathin structure and inimitable electronic band structures with unique functionalities, including indirect-to-direct band-gap transition [4], semiconductor-to-metal phase engineering [5], the large excitonic effect [6], and nondegenerate doping [7]. Furthermore, both MoS_2 and WS_2 have a light absorption coefficient that is about one order of magnitude higher than that of conventional 3-D semiconductor Si [8].

The short-circuit current density (J_{sc}), which is the maximum current that can be extracted from a PV device, is 0.1 mA/cm^2 for 1-nm-thick Si [8]. In contrast, a single-layer MoS_2 and WS_2 that is less than 1-nm thickness has a J_{sc} of 3.9 and 2.3 mA/cm^2, respectively [8]. Furthermore, the solar cell devices built through absorption-limited monolayer 2-D material junctions such as MoS_2/graphene-based Schottky junctions [9], [10] or MoS_2/WS_2-based excitonic solar cells [11] exhibit low efficiencies, imposing challenges for large-scale integrations [3]. To avoid low efficiency due to absorption-limited 2-D/2-D (graphene/MoS_2) monolayer junctions and high cost involved in fabrication of 3-D/3-D (p-Si/n-Si) bulk junctions, another avenue of integrating 2-D layers with 3-D bulk semiconductors (i.e., 2-D/3-D material junctions) has evolved. For example, 2-D/3-D heterojunctions, including high-efficiency graphene/Si [12] and MoS_2/Si [3] solar devices, have been recently reported. Such devices are primarily realized via micromechanical or chemical exfoliation [13] or transfer techniques [14], which are believed to modify the intrinsic properties of the graphene or TMD layers. However, the large-scale production of direct and transfer-free WS_2-on-Si (2-D/3-D) heterojunction solar cell devices is still a challenge.

Here, we report a scalable, reproducible, single-step CVD process for the fabrication of large-area WS_2 films on p-Si substrates under optimized conditions [Figure 1(a) and (b)]. The formation of thin WS_2 films were confirmed via Raman and X-ray photoelectron spectroscopic analysis. Owing to the n-type conductivity of WS_2 [15], it exhibits good
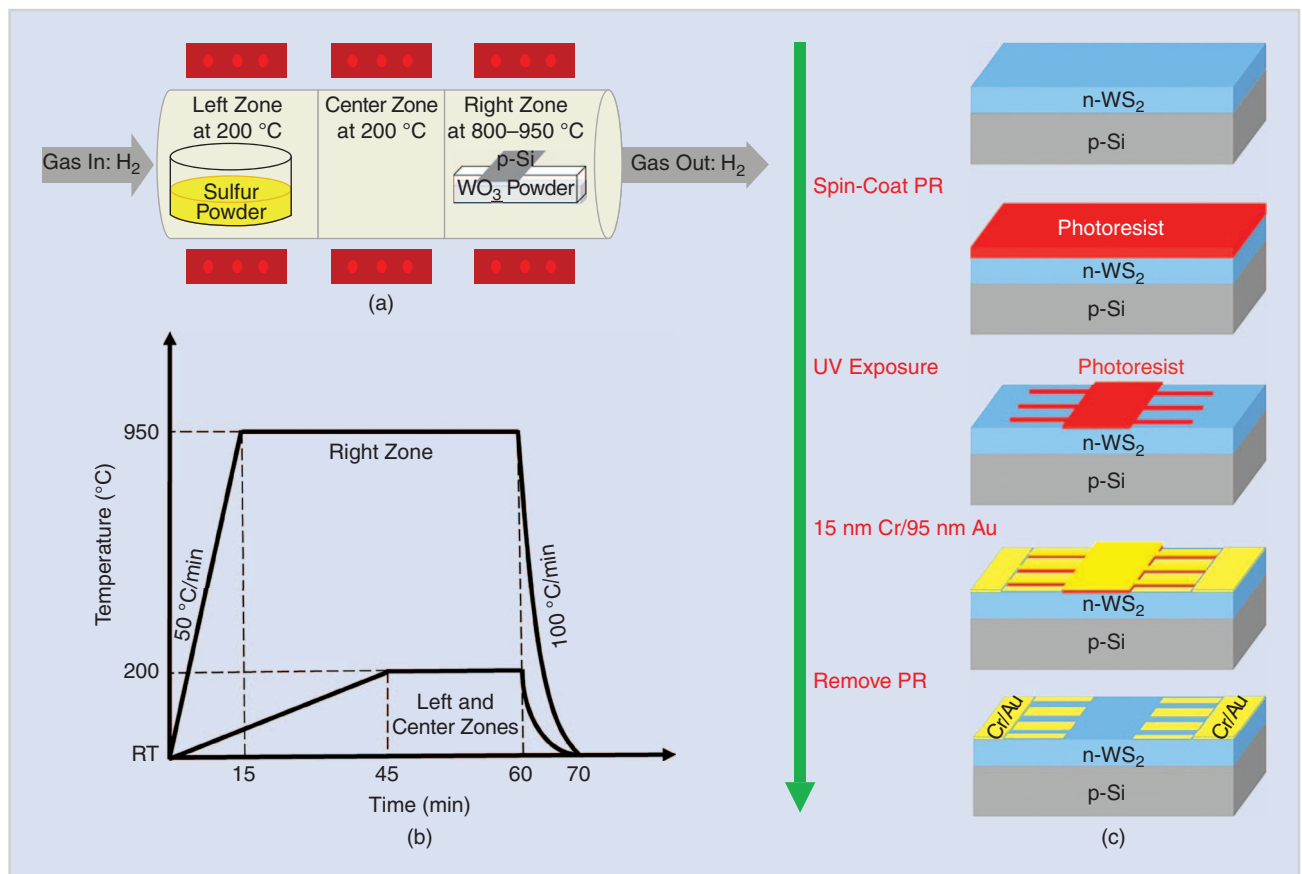

FIGURE 1 (a) The schematic of the CVD setup for the synthesis of WS_2. (b) The temperature versus time CVD thermal processing steps in different heating zones. (c) The lift-off photolithography process steps to fabricate WS_2/Si solar cell devices. RT: room temperature.

photoresponse under air mass 1.5 global (AM 1.5G) illumination when interfaced with a p-Si bulk semiconductor. Furthermore, the wavelength-dependent quantum efficiency measurements reveal the dominant recombination mechanisms controlling the device performance.

METHODS

The WS_2 thin films were synthesized on p-Si solar grade substrates via a three-zone low-pressure CVD [16] (MTI Corporation, Richmond, California) setup, as shown in Figure 1(a). Here, 20 mg sulfur (S) powder and 10 mg tungsten oxide (WO_3) powder were used as precursors, and hydrogen (H_2) at a flowrate of 15 standard cubic centimeter per minute was used as carrier gas. The chamber pressure was maintained at 100 mTorr. The S powder in the crucible was placed upstream (left zone) of the CVD system and heated to 200 °C in 45 min, then held at that temperature for 15–30 min. The WO_3 powder in the crucible was placed downstream (right zone) and heated to 800–950 °C in 15 min and then held at that temperature for 45–60 min. The p-Si chip was placed facedown on top of the crucible, which contained WO_3 powder in the right zone [Figure 1(a)]. The center zone of the CVD furnace was kept in the same condition as the left zone. The CVD thermal processing steps are described in Figure 1(b). The synthesized thin films of WS_2 were characterized by confocal Raman-spectroscopy (WITec alpha 300 Raman-AFMA with a laser wavelength of 532 nm) at room temperature in air and X-ray photoelectron spectroscopy (XPS) (Kratos AXIS-165) at room temperature in a vacuum, which is discussed in the next section.

For the solar cell device fabrications, the standard clean room microfabrication and metallization techniques were employed, including ultraviolet (UV) photolithography (Karl Suss MA6) and electron beam evaporation (Varian). The solar cell devices were fabricated by lift-off photolithography process steps, as outlined in Figure 1(c). Photoresist (PR, OIR 906-12) was spin-coated on the surface of WS_2/p-Si at 4,000 r/min for 45 s followed by baking at 110 °C for 1 min. The uniform pattern was created after exposing the PR to UV light (900 W). Furthermore, the chips were developed using OPD-4262 developer solution for 1 min. Subsequently, chromium (Cr, 10 nm) was deposited on the patterned PR followed by gold (Au, 95 nm) using electron beam evaporation. Finally, the PR and Cr/Au contacts on top of the PR were removed using acetone, leaving a patterned structure behind. A thin layer of silver (Ag) was deposited as a back-contact electrode for the WS_2/p-Si heterojunction solar cell devices. The PV and spectral responses of the final devices were recorded via a solar simulator (Sciencetech Inc., London, Ontario) of one sun at AM 1.5G illumination and a quantum efficiency measurement unit (ORIEL Instruments), respectively.
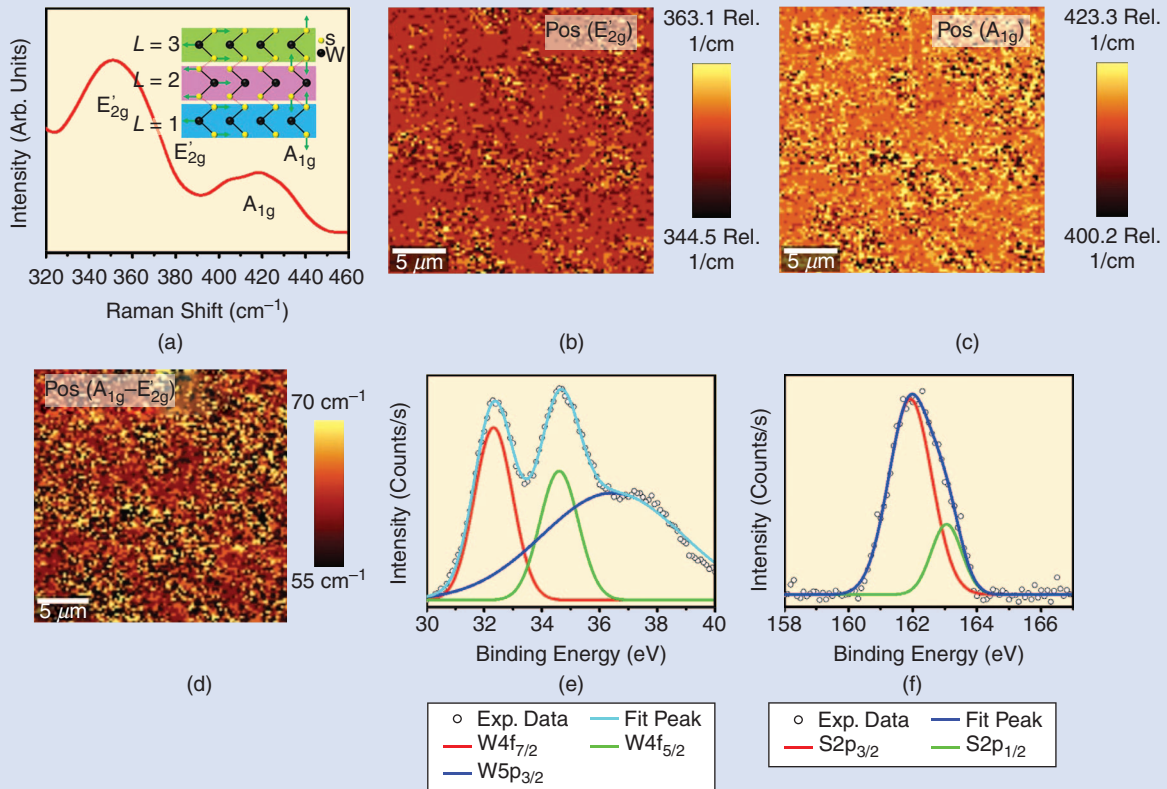

FIGURE 2 (a) The Raman spectrum of CVD-grown WS_2 on p-Si surfaces, with the schematic of atomic vibrations corresponding to E'_{2g} and A_{1g} modes shown in the inset; the Raman position mapping for (b) E'_{2g}, (c) A_{1g}, and (d) $(A_{1g} - E'_{2g})$ peak position difference; and the high-resolution XPS spectra for (e) W 4f and (f) S 2p core levels. Arb.: arbitrary; Rel.: relative; Exp.: experimental.

RESULTS AND DISCUSSION

Scanning Raman spectroscopy was employed to determine the coverage, continuity, and quality of the CVD-grown WS_2 layers [17]. The WS_2 nominally exhibits two signature Raman vibrational modes, as shown in Figure 2(a): one is the in-plane vibrational mode (E'_{2g}), and the other is the out-of-plane vibrational mode (A_{1g}). Figure 2(a) shows that the E'_{2g} peak is centered at 351.7 cm^{-1} and the A_{1g} peak is centered at 418.8 cm^{-1}, indicating a peak position difference of about 67 cm^{-1}, which corresponds to a few layers of WS_2 film. The inset of Figure 2(a) shows the schematic of tungsten (W) and S atomic vibrations for E'_{2g} and A_{1g} Raman modes. Furthermore, the Raman position mappings of E'_{2g} [Figure 2(b)] and A_{1g} [Figure 2(c)] modes affirm the formation of continuous WS_2 films on p-Si surfaces. It is also observed from the mapping of the position difference between A_{1g} and E'_{2g} in Figure 2(d) that the CVD-grown WS_2 film is nearly uniform in thickness over the entire p-Si substrates.

XPS was used to determine the chemical composition and stoichiometry of the CVD-grown WS_2 films. The XPS spectrum for W and S core levels are deconvoluted via a Gaussian function. Figure 2(e) presents the core energy levels for W; i.e., W $4f_{7/2}$, W $4f_{5/2}$, and W $5p_{3/2}$ centered at binding energies (E_B) of 32.32, 34.59, and 36.45 eV, respectively, which correspond to the four or more valence states of W in the synthesized WS_2 films [18], [19]. Figure 2(f) depicts the doublet peaks; i.e., S $2p_{3/2}$ and S $2p_{1/2}$ for S 2p at E_B of 161.9 and 163.05 eV, respectively, which correspond to the S–W bonding [18], [19]. However, the atomic ratio between W and S is 1:1.24, which suggests that the synthesized WS_2 films exhibit S deficiency. The formation of elemental nonstoichiometric WS_2 films may be ascribed to various factors, such as the partial reduction of WO_3 powder in the H_2 environment and/or the formation of some undesired products; i.e., WO_xS_x in the synthesized films [19].

To characterize the PV response of the WS_2/p-Si heterojunction, the solar cell devices were fabricated through a lift-off photolithography process [as mentioned in the "Methods" section; see Figure 1(c)]. Figure 3(a) shows the schematic of the WS_2/p-Si solar cell device structure. The optical images of the solar cell device are presented in Figure 3(b). The electrical characterizations for the WS_2/p-Si heterojunction devices were carried out by a Keithley 2612 source meter unit (SMU). The nonlinear current density versus voltage (LnJ-V) characteristics [Figure 3(c)] for the device under dark indicates the
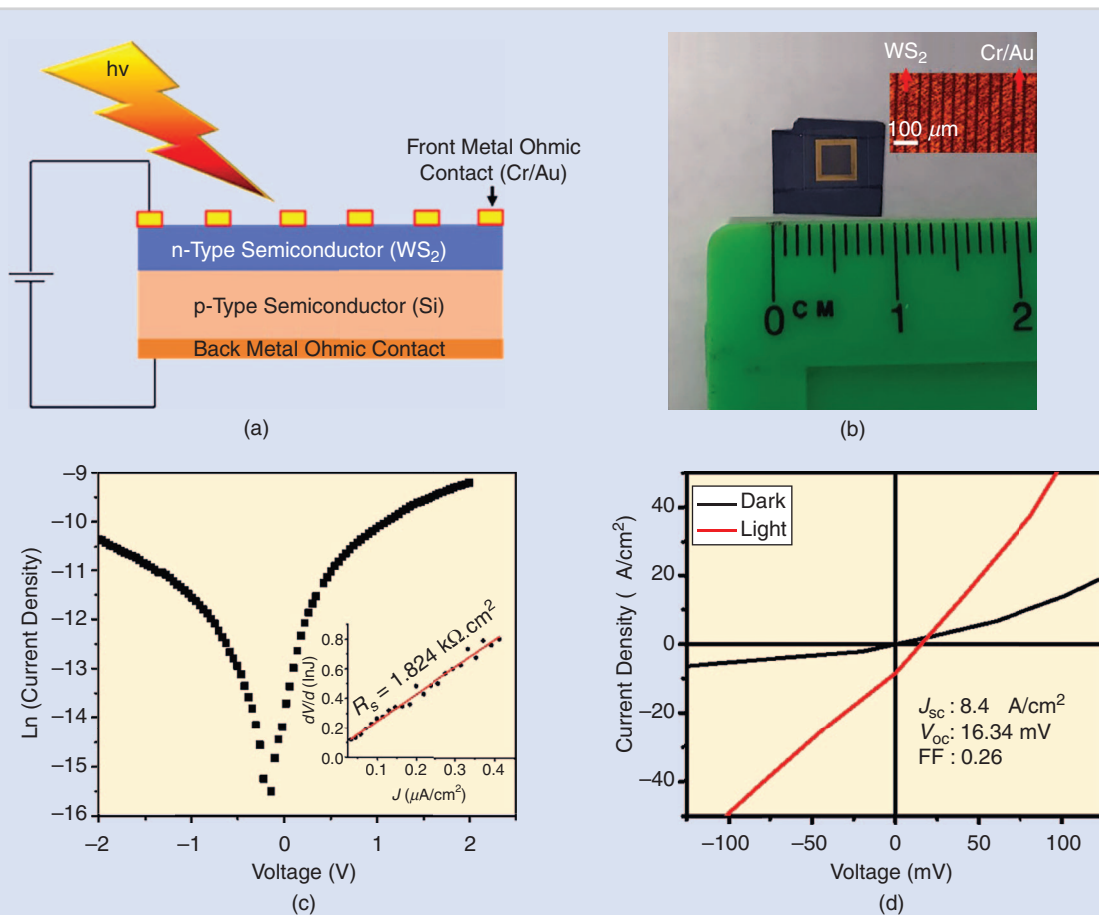

FIGURE 3 The (a) schematic and (b) optical image of the WS_2/p-Si solar cell device structure; (c) the nonlinear dark Ln(J)-V characteristics, with the dV/d(LnJ) versus the J profile shown in the inset; and (d) the light and dark J-V characteristics, with the PV parameters shown in the inset. A: ampere.

formation of a diodic P–N junction between the n-WS$_2$ 2-D layer and the p-Si 3-D bulk semiconductor. The series resistance of the device is 1.824 kΩ.cm^2, which is determined from the slope of dV/d(LnJ) versus J curve [inset of Figure 3(c)] under dark conditions [12].

Figure 3(d) presents the PV characteristics of the WS$_2$/p-Si heterojunction solar cell device with (red J–V curve) and without (black curve) exposure to AM 1.5G illumination. The black curve represents the nonlinear diodic dark characteristics of the device. A typical light J–V PV curve provides values of J$_{sc}$, open-circuit voltage (V$_{oc}$), and FF. The WS$_2$/p-Si solar cell device exhibits the following PV characteristics: J$_{sc}$ of 8.4 μA/cm^2, V$_{oc}$ of 16.34 mV, and FF of ~26%. The origin of low PV characteristics has been further investigated via the measurement of photoresponse and the quantum efficiency of the

device as discussed in the next section, which provides the avenues to improve the device performances.

The WS$_2$/p-Si heterojunction device was investigated for photoexcitation at an applied bias of 1 V. A prominent photoresponsivity was observed and is presented in Figure 4(a). However, an immediate decrease of photocurrent was observed after blocking incident simulated sunlight (off status), as presented in Figure 4(b). An external bias of 1 V was applied to the WS$_2$/p-Si heterojunction device, because photogenerated charge carriers (electron–hole pairs) in the WS$_2$ layer were able to drift faster as per the equation $v_d = \mu E$ and collected by the respective metal electrode contacts.

Curve fitting of the decay signal to an exponential function $(I = I_0 e^{-\frac{t}{\tau}})$ provides a time constant (τ) of 264 ms. Such a rapid decay of photocurrent can

be attributed to the relaxation of charge carriers via recombination [20]. To further confirm the effect of recombination over the entire WS$_2$/p-Si device thickness on the solar cell performance, the EQE is measured at different wavelengths of incident light. The EQE measurement setup consists of a Xenon lamp, a monochromator, and a Keithley 2612 SMU to measure the current response of the device [Figure 4(c)] [21], [22]. The spectral dependence of the EQE (EQE versus wavelength profile) of the WS$_2$/p-Si heterojunction device is shown in Figure 4(d).

The EQE is about 15–25% for blue and green light, which may be attributed to the fact that 1) the higher front surface recombination in the blue region of the light affects carriers generated near the front surface and 2) a low diffusion length or high bulk recombination will affect the collection probability from the solar cell bulk
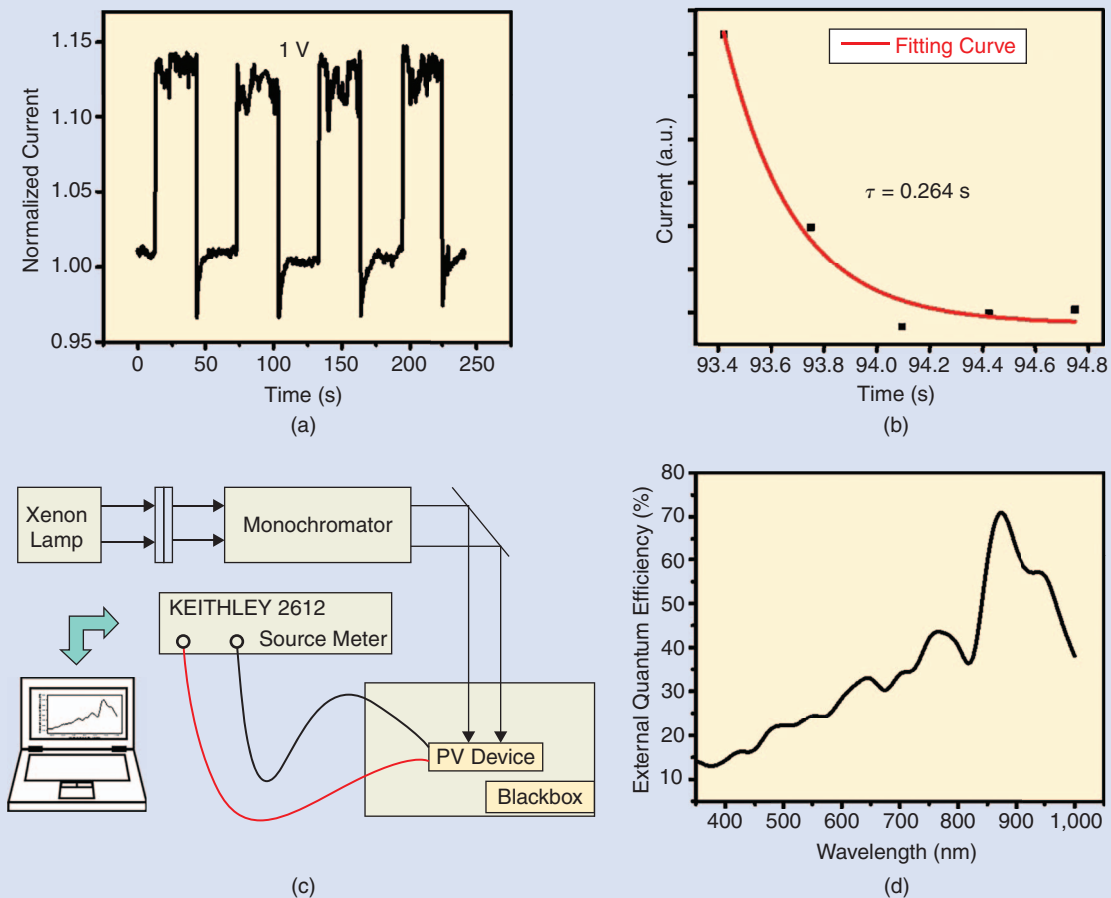

FIGURE 4 The WS$_2$/p-Si heterojunction. (a) The photoresponse characteristics, (b) the photocurrent decay, (c) the quantum efficiency measurement setup, and (d) the EQE versus the wavelength profile.

and reduce the EQE in the green portion of the spectrum, as the green light is nominally absorbed in the solar cell bulk. The high EQE response in the red and far-IR regions indicates that the charge carriers generated at the rear of the device are able to transport to the junction. This may be due to the high absorption coefficient of the CVD-grown semiconducting WS_2 films [23], [24].

CONCLUSION

Continuous, large-area, semiconducting 2-D WS_2 thin films are synthesized on 3-D p-Si solar grade substrates via a three-zone low-pressure chemical vapor deposition system and characterized via scanning Raman and XPS spectroscopy. These WS_2/p-Si type-II heterojunction devices exhibited good PV and spectral responses. The PV devices are fabricated via a standard lift-off photolithography process, with Cr/Au as the top Ohmic metal contact electrode and Ag as the back Ohmic metal contact electrode. The device exhibited a J_{SC} of 8.4 μA/cm^2, a V_{OC} of 16.34 mV, and a FF of 26% when tested under AM 1.5G illumination.

The photoresponse and spectral responses of the solar device provide information on trapped states and the recombination profile over the entire device thickness. In the future, we envision the evolution of next-generation complex TMD structures with stoichiometric composition, improved passivation, and plasmonics amplification.

ABOUT THE AUTHORS

Sanjay Behura (sbehura1@uic.edu) is with the Department of Chemical Engineering, University of Illinois at Chicago.

Kai-Chih Chang (oldbigbaek@hotmail.com) is with the Department of Chemical Engineering, University of Illinois at Chicago.

Yu Wen (ywen20@uic.edu) is with the Department of Chemical Engineering, University of Illinois at Chicago.

Rousan Debbarma (rdebba2@uic.edu) is with the Department of Chemical Engineering, University of Illinois at Chicago.

Phong Nguyen (tuanphong2208@gmail.com) is with the Department of Chemical Engineering, University of Illinois at Chicago.

Songwei Che (sche4@uic.edu) is with the Department of Chemical Engineering, University of Illinois at Chicago.

Shikai Deng (sdeng8@uic.edu) is with the Department of Chemical Engineering, University of Illinois at Chicago.

Michael R. Seacrist (MSeacrist@sunedisonsemi.com) is with SunEdison Semiconductor, Saint Peters, Missouri.

Vikas Berry (vikasb@uic.edu) is with the Department of Chemical Engineering, University of Illinois at Chicago.

REFERENCES

[1] W. Shockley and H. J. Queisser. "Detailed balance limit of efficiency of p-n junction solar cells," *J. Appl. Phys.*, vol. 32, no. 3, pp. 510–519, Mar. 1961.

[2] X. Li, H. Zhu, K. Wang, A. Cao, J. Wei, C. Li, Y. Jia, Z. Li, X. Li, and D. Wu, "Graphene-on-silicon schottky junction solar cells," *Adv. Mater.*, vol. 22, no. 25, pp. 2743–2748, Apr. 2010.

[3] M. L. Tsai, S.-H. Su, J.-K. Chang, D.-S. Tsai, C.-H. Chen, C.-I. Wu, L.-J. Li, L.-J. Chen, and J.-H. He, "Monolayer MoS$_2$ heterojunction solar cells," *ACS Nano.*, vol. 8, no. 8, pp. 8317–8322, Aug. 2014.

[4] Q. H. Wang, K. Kalantar-Zadeh, A. Kis, J. N. Coleman, and M. S. Strano, "Electronics and optoelectronics of two-dimensional transition metal dichalcogenides," *Nanotechnol.*, vol. 7, pp. 699–712, Nov. 2012.

[5] D. Voiry, A. Mohite, and M. Chhowalla, "Phase engineering of transition metal dichalcogenides," *Chem. Soc. Rev.* vol. 44, no. 9, pp. 2702–2712, 2015.

[6] M. M. Ugeda, A. J. Bradley, S.-F. Shi, F. H. da Jornada, Y. Zhang, D. Y. Qiu, W. Ruan, S.-K. Mo, Z. Hussain, Z.-X. Shen, F. Wang, S. G. Louie, and M. F. Crommie, "Giant band gap renormalization and excitonic effects in a monolayer transition metal dichalcogenide semiconductor," *Nat. Mater.*, vol. 13, no. 12, pp. 1091–1095, 2014.

[7] S. Behura and V. Berry, "Interfacial nondegenerate doping of MoS$_2$ and other two-dimensional semiconductors," *ACS Nano.*, vol. 9, no. 3, pp. 2227–2230, 2015.

[8] M. Bernardi, M. Palummo, and J. C. Grossman, "Extraordinary sunlight absorption and one nanometer thick photovoltaics using two-dimensional monolayer materials," *Nano Lett.*, vol. 13, no. 8, pp. 3664–3670, 2013.

[9] W. Zhang, C.-P. Chuu, J.-K. Huang, C.-H. Chen, M.-L. T., Y.-H. Chang, C.-T. Liang, Y.-Z. Chen, Y.-L. Chueh, J.-H. He, M.-Y. Chou, and L.-J. Li, "Ultrahigh-gain photodetectors based on atomically thin graphene-MoS$_2$ heterostructures," *Sci. Rep.* vol. 4, 2014.

[10] Y. Tsuboi, F. Wang, D. Kozawa, K. Funahashi, S. Mouri, Y. Miyauchi, T. Takenobub, and K. Matsuda, "Enhanced photovoltaic performances of graphene/Si solar cells by insertion of a MoS$_2$ thin film," *Nanoscale*, vol. 7, no. 34, pp. 14476–14482, 2015.

[11] L. Y. Gan, Q. Zhang, Y. Cheng, and U. Schwingenschlögl, "Photovoltaic heterojunctions of fullerenes with MoS$_2$ and WS$_2$ monolayers," *J. Phys. Chem. Lett.*, vol. 5, no. 8, pp. 1445–1449, 2014.

[12] X. Miao, S. Tongay, M. K. Petterson, K. Berke, A. G. Rinzler, B. R. Appleton, and A. F. Hebard. "High efficiency graphene solar cells by chemical doping," *Nano Lett.*, vol. 12, no. 6, pp. 2745–2750, 2012.

[13] G. Eda, H. Yamaguchi, D. Voiry, T. Fujita, M. Chen, and M. Chhowalla, "Photoluminescence from chemically exfoliated MoS$_2$," *Nano Lett.*, vol. 11, no. 12, pp. 5111–5116, 2011.

[14] T. Georgiou, R. Jalil, B. D. Belle, L. Britnell, R. V. Gorbachev, S. V. Morozov, Y.-J. Kim, A. Gholinia, S. J. Haigh, O. Makarovsky, L. Eaves, L. A. Ponomarenko, A. K. Geim, K. S. Novoselov, and A. Mishchenko, "Vertical field-effect transistor based on graphene-WS$_2$ heterostructures for flexible and transparent electronics," *Nat Nanotechnol.*, vol. 8, no. 2, pp. 100–103, 2013.

[15] X. Duan, C. Wang, J. C. Shaw, R. Cheng, Y. Chen, H. Li, X. Wu, Y. Tang, Q. Zhang, A. Pan, J. Jiang, R. Yu, Y. Huang, and X. Duan, "Lateral epitaxial growth of two-dimensional layered semiconductor heterojunctions," *Nat Nanotechnol.*, vol. 9, no. 12, pp. 1024–1030, 2014.

[16] S. Behura, P. Nguyen, S. Che, R. Debbarma, and V. Berry, "Large-area, transfer-free, oxide-assisted synthesis of hexagonal boron nitride films and their heterostructures with MoS$_2$ and WS$_2$," *J. Am. Chem. Soc.*, vol. 137, no. 40, pp. 13060–13065, 2015.

[17] A. Berkdemir, H. R. Gutiérrez, A. R. Botello-Méndez, N. Perea-López, A. L. Elías, C.-I. Chia, B. Wang, V. H. Crespi, F. López-Urías, J.-C. Charlier, H. Terrones, and M. Terrones, "Identification of individual and few layers of WS$_2$ using Raman spectroscopy," *Sci. Rep.*, vol. 3, 2013.

[18] X. Mao, Y. Xu, Q. Xue, W. Wang, and D. Gao, "Ferromagnetism in exfoliated tungsten disulfide nanosheets," *Nanoscale Res. Lett.*, vol. 8, p. 430, Oct. 2013.

[19] K. M. McCreary, A. T. Hanbicki, G. G. Jernigan, J. C. Culbertson, and B. T. Jonker, "Synthesis of large-area WS$_2$ monolayers with exceptional photoluminescence," *Sci. Rep.*, vol. 6, 2016.

[20] B. Li, G. Shi, S. Lei, Y. He, W. Gao, Y. Gong, G. Ye, W. Zhou, K. Keyshar, J. Hao, P. Dong, L. Ge, J. Lou, J. Kono, R. Vajtai, and P. M. Ajayan, "3D band diagram and photoexcitation of 2D-3D semiconductor heterojunctions," *Nano Lett.*, vol. 15, no. 9, pp. 5919–5925, 2015.

[21] American Society for Testing and Materials, "ASTM Standard Test Method for Spectral Responsivity Measurements of Photovoltaic Devices," Philadelphia, PA, 2013. doi:10.1520/E1021-12.

[22] C. F. Lin, M. Zhang, S. W. Liu, T. L. Chiu, and J. H. Lee, "High photoelectric conversion efficiency of metal phthalocyanine/fullerene heterojunction photovoltaic device," *Int. J. Mol. Sci.*, vol. 12, no. 1, pp. 476–505, 2011.

[23] A. Jager-Waldau, M. C. Lux-Steiner, and E. Bucher, "WS$_2$ thin films a new candidate for solar cells," in *Proc. Photovoltaic Specialists Conf.*, June 1993, pp. 597–602.

[24] A. R. Beal, J. C. Knights, and W. Y. Liang, "Transmission spectra of some transition metal dichalcogenides. II. Group VIA: trigonal prismatic coordination," *J. Phys. C Solid State Phys.*, vol. 5, no. 24, pp. 3540–3551, 1972.

N